Sustainable Cities and Society 25 (2016) 1–12

Contents lists available at ScienceDirect

Sustainable Cities and Society

journal homepage: www.elsevier.com/locate/scs

The impact of urban planning strategies on heat stress in a climate-change perspective

Fredrik Lindberg*, Sofia Thorsson, David Rayner, Kevin Lau

University of Gothenburg, Göteborg Urban Climate Group, Earth Science Centre, Box 460, SE-405 30 Göteborg, Sweden

ARTICLE INFO

Article history:
Received 15 September 2015
Received in revised form
17 December 2015
Accepted 7 April 2016
Available online 16 April 2016

Keywords:
Göteborg
Sweden
Vegetation
Statistical downscaling
Spatial variability
Mean radiant temperature

ABSTRACT

Spatial and temporal characteristics of outdoor heat stress for a redevelopment area in Gothenburg, Sweden, in a climate change perspective, using mean radiant temperature (T_{mrt}) as a proxy for heat stress is presented. The impact of climate change on T_{mrt} was evaluated using statistically downscaled data from a regional climate model. The simulated average T_{mrt} for the future scenarios was not higher than for today's climate, because the increased longwave radiation fluxes caused by higher temperatures were offset by reduced shortwave radiation fluxes caused by increased cloudiness. The spatial pattern of T_{mrt} in the study area during warm and clear weather is primarily governed by the shadow patterns of buildings and vegetation. The highest average-daytime T_{mrt} was found at open locations, but because open areas also have the highest frequency of sunlit occasions, this does not necessarily imply that open areas are most prone to heat-stress. When considering only occasions during clear and warm weather situations, the highest T_{mrt} were usually found close to sun-exposed, south-facing walls. Under these criteria, denser urban environments have lower heat stress than more open urban environments. The warmest areas were also found to be the warmest areas in the future as well.

Tree-shadows are an effective measure to reduce daytime T_{mrt}. Trees was found to have the largest impact on T_{mrt} in open areas where vegetation is sparse, especially when the distance to the nearest "cool" place is used as a measure of heat-stress.

© 2016 Elsevier Ltd. All rights reserved.

1. Introduction

If the increasing global anthropogenic greenhouse gas emission rates are not countered by mitigating actions, global mean surface temperatures are likely to rise by 1.4–4.8 °C by 2100 (IPCC, 2007). Under such scenarios, heat wave episodes will become more frequent, more intense, and longer lasting (Meehl & Tebaldi, 2004). Climate change could magnify the urban heat island effect in some locations (McCarthy, Best, & Betts, 2010), and such changes would affect urban populations directly by changing human thermal comfort through heat stress and cold stress. Establishing urban-planning guidelines to reduce heat and cold stress can help lessen the negative effects of climate change, and they can take advantage of the opportunities that climate change presents to help create healthy and sustainable cities.

A number of predictors can be used to evaluate heat stress. The most commonly used predictor is the air temperature (T_a), and this is sometimes adjusted for humidity to give the apparent temperature or for wind speed to give the wind-chill index. Also available are various thermal indices, such as physiologically equivalent temperature (PET, Mayer and Höppe, 1987) and the universal thermal climate index (UTCI, e.g. Fiala, Havenith, Bröde, Kampmann, & Jendritzky, 2012), both of which take into account relevant meteorological parameters (air temperature, air humidity, wind speed, and mean radiant temperature) as well as thermo-physiological elements (clothing, activity, age, etc.).

The mean radiant temperature (T_{mrt}) is directly influenced by urban geometry and surface material, and this makes it a good measure to identify urban hot spots. On clear and calm summer days, T_{mrt} is the most important meteorological parameter influencing human energy balance and heat load (Ali-Toudert & Mayer, 2007; Mayer and Höppe, 1987), and T_{mrt} has been shown to be a good predictor of both heat stress and heat-related mortality (Thorsson et al., 2014). T_{mrt} is defined as the 'uniform temperature of an imaginary enclosure in which the radiant heat transfer from the human body equals the radiant heat transfer in the actual non-uniform enclosure' (ASHRAE, 2001). It describes the radiative exchange between a person and their environment and includes the effects of air temperature, surface temperature, and solar radiation. Whereas intra-urban T_a differences are rather small during the day, T_{mrt}

* Corresponding author.
E-mail address: fredrikl@gvc.gu.se (F. Lindberg).

http://dx.doi.org/10.1016/j.scs.2016.04.004
2210-6707/© 2016 Elsevier Ltd. All rights reserved.

shows large spatial variations over short distances (Emmanuel & Fernando, 2007; Lindberg & Grimmond, 2011; Mayer, Holst, Dostal, Imbery, & Schindler, 2008; Thorsson, Lindberg, Bjorklund, Holmer, & Rayner, 2011). These variations are mainly governed by shadow patterns generated by trees, buildings, and topography and to a lesser extent by differences in the thermal and radiative properties of the surrounding surface materials, i.e., albedo, emissivity, and heat capacity.

During clear summer days with high solar irradiance, the highest T_{mrt} is found in areas near sunlit walls at noon or early afternoon. These locations experience high levels of direct and reflected shortwave radiation as well as long-wave radiation from wall surfaces exposed to the sun (Lindberg, Holmer, Thorsson, & Rayner, 2013). As a result, T_{mrt} can be substantially higher than T_a. At night, when shortwave radiation is absent, T_{mrt} is similar to T_a.

Global Climate Models (GCMs) are the best tools we currently have for estimating the effect of increased greenhouse gas concentrations on the global climate. Changes at sub-continental scales are commonly assessed by using GCM outputs as inputs into higher-resolution Regional Climate Models (RCMs). However, even RCM outputs are biased compared to local climate records, and care is required when using RCM outputs to estimate the combined effect of changes in several meteorological parameters on heat stress. Possible approaches include converting observation-based threshold values into percentiles (Muthers, Matzarakis, & Koch, 2010), historical-resampling whereby progressively warmer days from the historical record are selected to represent the climate of the future (Thorsson et al., 2011), and modifying observed meteorological data based on the changes between a present-day period and a future period in an RCM simulation (Rayner, Lindberg, Thorsson, & Holmer, 2014).

Although concerns about future heat stress are focused on southern of Europe where summer air temperatures are already high, the predicted increase in heat in Scandinavia must also be taken seriously (Rocklov & Forsberg, 2008). According to the Swedish government's report 'Sweden facing climate change—threats and opportunities' (SOU, 2007), the number of heat-related deaths in the Stockholm area in the summer could rise by 5% if the air temperature rises by 4 °C during summer. The same report estimates that the increased costs of heat-related deaths due to climate change could be €50–70 billion in Sweden from 2010 to 2100. Although the number of cold-related deaths is expected to decrease due to milder winters, the risks associated with heat waves might be greater because the northern populations have had a long time to adapt to long periods of extreme cold but have yet to adapt to the occurrence of hot periods (Oudin Åström, Forsberg, Ebi, & Rocklöv, 2013).

The purpose of this paper is to examine the temporal and spatial characteristics of outdoor heat stress for a redevelopment area in Gothenburg, Sweden, in a climate change perspective using T_{mrt} as a proxy for heat stress. The specific objectives are to examine:

- how different urban-planning proposals regarding building density and vegetation cover (trees and bushes) influence the temporal and spatial characteristics of T_{mrt}.
- the impact of climate change on T_{mrt} in the study area using statistically downscaled data from an RCM.

This study is a part of the larger research project 'Adapting cities to climate induced risks' that aims to develop methods and knowledge for reducing the risks and effects of extreme weather under a changed climate (e.g. Jonsson & Lundgren, 2014; Konarska, Lindberg, Larsson, Thorsson, & Holmer, 2014; Lindberg et al., 2013; Rayner et al., 2014; Thorsson et al., 2014). The project addresses the risks of high temperatures, poor air quality, landslides, and flooding. The project brings together researchers with specialist expertise within several fields – including measuring and modeling outdoor thermal comfort, air quality, natural disaster risk assessment, socioeconomic analysis, multi-criteria analysis, and urban planning – and includes both stakeholders and practitioners.

2. Methods

2.1. Study area – Frihamnen

The free-port area (*Frihamnen*) located by the river (*Göta älv*) in Gothenburg, Sweden, was selected as the case study area (Fig. 1). The area will soon be transformed from an industrial dockland into a modern residential and commercial area. The area is low-lying and relatively flat and covers around 85 ha (the area inside the red line in Fig. 1). The area currently consists of three large piers and adjacent harbors and the surrounding land on two sides.

Two planning strategies focusing on climate adaptation were used in this study. The first, called *defense* (Fig. 2a), had a larger plot to area ratio, whereas *retreat* (Fig. 2b) was a less dense planning strategy. The two adaptation alternatives describe the strategies for coping with the threat of flooding, which is already a hazard in the area today. In the *retreat* strategy, the three existing piers are left relatively unmanaged and are intended to be used for recreation, sea and land sports, music, and other large events as well as to provide green park space. In this proposal, buildings are only allowed on the adjacent, non-flood-prone land areas. A maximum of 600,000 m^2 of apartment area would be allowed under such strategy. In the *defend* planning proposal, the area is protected by a permanent barrier with an operable gate (i.e., a resistance strategy), and buildings are also allowed on the piers and in the present-day harbors. The total area that can be built on is 1,200,000 m^2 (Fig. 2b), which is twice that available in the *retreat* strategy.

In addition to the *retreat* and *defend* planning strategies, three different vegetation proposals were examined in this study. Vegetation in this context implies objects that can create shade – such as trees and bushes – and grass and low shrubs are not considered. The first vegetation proposal is for no vegetation at all. The second proposal is for 'conventional' vegetation cover, that is, vegetation similar to other parts of central Gothenburg. The third vegetation strategy includes abundant vegetation throughout the study area. The vegetation proposals were generated by expert judgment (see the acknowledgements). The second and the third vegetation strategies are shown in Fig. 2. Descriptive data for the different planning proposals are presented in Table 1.

2.2. Meteorological observations

Hourly air temperature records were obtained from the Swedish Meteorological and Hydrological Institute (SMHI) for climate stations 7141 (years 1983–1999) and 7142 (years 1999–2006), both of which are located inside the city of Gothenburg. Missing records were filled using observations from Gothenburg City Airport, approximately 10 km northwest of the city center. Hourly solar radiation data (global and diffuse components) were obtained for SMHI station 92513, which is located on the 7-story building *Ellysepalatset* in Gothenburg at a height of approximately 23 m above sea level. Global and diffuse solar radiation was measured with a Kipp and Zonen pyranometer, and direct solar radiation was calculated explicitly from the difference between the global and diffuse components.

2.3. Climate scenarios

The climate scenarios used in this project were based on outputs from the ECHAM5/MPI-OM GCM (Roeckner et al., 2003) forced with the SRES A1B greenhouse-gas emission scenario and downscaled to

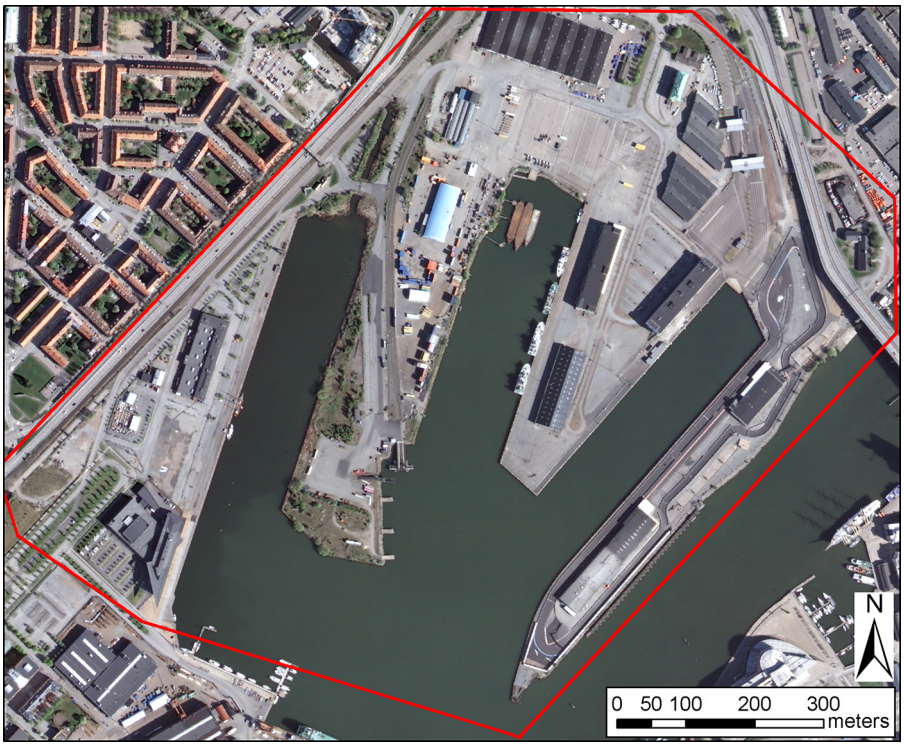

Fig. 1. Overview of Frihamnen in Gotenburg, Sweden. The red line shows the borders of the area of interest in this study. (For interpretation of the references to colour in this figure legend, the reader is referred to the web version of this article.)

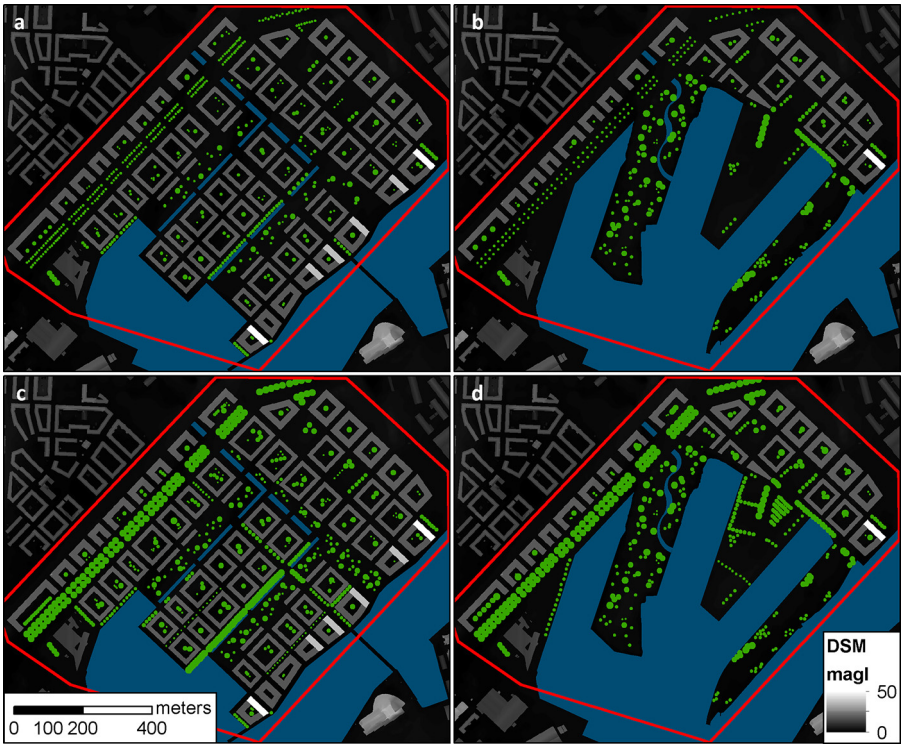

Fig. 2. The different planning strategies used in this study. (a) *Defend* with conventional vegetation cover. (b) *Retreat* with conventional vegetation cover. (c) *Defend* with abundant (increased) vegetation cover. (d) *Retreat* with abundant (increased) vegetation cover. The colors blue and green represent the location of water and trees, respectively. The red line shows the borders of the area of interest. DSM = Digital Surface Model, magl = m above ground level. (For interpretation of the references to colour in this figure legend, the reader is referred to the web version of this article.)

25-km resolution with the RCA3 regional climate model (Kjellström et al., 2005). The SRES A1 scenario describes rapid, global economic development, and summer temperatures in Northern Europe are expected to increase by at least 2 °C by 2100 if greenhouse gas emissions follow the SRES A1B scenario (Meehl et al., 2007). The A1B scenario corresponds to a 'mid-range' reference-scenario (that is, a

Table 1
Surface characteristics for the different planning proposals used in this study.

	Retreat			Defend		
	Vegetation strategy			Vegetation strategy		
	None	Conventional (current)	Abundant	None	Conventional	Abundant
Building fraction	13.8%	13.8%	13.8%	26.0%	26.0%	26.0%
Water fraction	57.9%	57.9%	57.9%	37.8%	37.8%	37.8%
Tree cover fraction	0.0%	3.0%	8.6%	0.0%	4.9%	10.8%
$z_{H(buildings)}$ (m)	10.8	10.8	10.8	9.1	9.1	9.1
$z_{H(vegetation)}$ (m)	NA	12.3	15.2	NA	14.0	15.2

scenario without deliberate greenhouse-gas mitigation actions) in the context of more recent scenario modeling (Moss et al., 2010). The following climate periods were used in this study: the current climate, the predicted mid-century climate (2040–2069), and the predicted end of century climate (2070–2099).

The climate-scenario data used as input for the T_{mrt} modeling were created from these RCM outputs by combining them with the meteorological observations of air temperature and 3-component solar radiation (global, diffuse, and direct) using the method of Rayner et al. (2014). With this method, change factors were first calculated from differences in ranked daily RCM outputs for a future period and a present-day period. Changes consistent with these daily factors were then applied to historical hourly meteorological observations to create future scenarios. A summary of the method is given here.

For air temperature, the hourly scenarios were created by interpolating the change factors for daily maximum and minimum air temperature. That is, for each day in the historical record, a change-factor for the daily maximum air temperature was determined from the ranked changes in the RCM maximum air temperature outputs. Change factors for the minimum air temperatures for each day were similarly determined. These series of change factors were then combined, and change factors for every hourly temperature value in the historical record were derived using linear interpolation.

For three-component radiation, the procedure was more complicated. This was firstly because the RCM outputs do not separate solar radiation into direct and diffuse components, and secondly because change factors need to be derived in such a way that the modified global, diffuse, and direct radiation remain self-consistent. In summary, change factors for daily global radiation were first calculated for each day in the historical record based on differences in ranked daily incoming shortwave radiation between the present-day RCM and scenario outputs. The change factor for daily global radiation was applied to all hourly global radiation values for that day. To calculate change factors for the hourly diffuse radiation values, the diffuse radiation was estimated from the global radiation using the method of Reindl, Beckman, and Duffie (1990) for both the observed and modified (future) hourly global radiation. The ratio of these estimates is the change factor to be applied to the observed historical diffuse radiation. Finally the direct radiation component for the scenario was determined from the modified global and diffuse radiation components.

The estimation of T_{mrt} in SOLWEIG (see below) is the most sensitive to T_a and shortwave radiation, whereas it is almost unaffected by air humidity. Thus, the climate scenarios used the unmodified observed hourly relative humidity.

2.4. Spatial and temporal modeling of T_{mrt}

This study used the SOLWEIG model (version 2013a, Lindberg 2012), which simulates the spatial variation of 3-D radiation fluxes and T_{mrt} as well as shadow patterns and sky view factors (SVFs) in complex urban settings. A detailed description of the SOLWEIG model, including the results from ground-truthing the model in different urban settings, weather conditions, and regional contexts, is given in Lindberg, Holmer, and Thorsson (2008) and Lindberg and Grimmond (2011). A summary follows here.

Spatial variations in T_{mrt} were calculated using the "full" SOLWEIG model. In this configuration, SOLWEIG requires the meteorological parameters of air temperature, relative humidity, and solar radiation (the global and diffuse components) together with a digital surface model (DSM) and a representative latitude/longitude for the location. The DSM represented ground and building heights, with a resolution of 2 m, had an extent of 599 × 683 pixels and was derived following Lindberg (2005). The effects of trees and bushes were modeled with vegetation included as a separate DSM layer (Lindberg & Grimmond, 2011). Albedo and emissivity for buildings and vegetation were 0.20 and 0.95, respectively (Oke, 1987). The transmissivity of shortwave and longwave radiation through vegetation was 5% and 0%, respectively (Lindberg & Grimmond, 2011). T_{mrt} was calculated for a standing person with the factors specifying the proportion of radiation received from each direction set to 0.22 for east, west, north, and south and to 0.06 for radiation fluxes from above and below. Absorption coefficients for shortwave and longwave radiation were 0.7 and 0.97, respectively (Höppe 1992; VDI, 1998). Nocturnal T_{mrt} is difficult to estimate because information on cloudiness (which affects the sky emissivity and incoming longwave fluxes) is lacking. Here, the cloudiness was extrapolated from late afternoon up until midnight, and cloudiness from midnight to sunrise was assumed to be the value of early morning. In this study, the methodology of Crawford and Duchon (1999) was used to estimate incoming longwave radiation. Neither wind fields nor variations in ground or building wall materials are considered in the current version of the model.

A simplified version of SOLWEIG, called SOLWEIG1D (Lindberg 2012), was used to examine how the radiant fluxes and T_{mrt} for a non-specific (generic) urban location might be affected by climate change. Unlike the full SOLWEIG simulations discussed above, where SVF and shadow patterns are determined for each pixel in a DSM, SOLWEIG1D has a single, fixed, user-specified SVF (here 0.6) that is supposed to represent a typical urban environment. The location is assumed to be sunlit during the daytime hours, which would not would be the case in a real-world situation where surrounding objects would block the sun at specific times of the day and year when SVF < 1.

2.5. Experimental configuration

SOLWEIG was run for each of the three climate periods (current climate, 2040–2069, and 2070–2099) with two different planning strategies (*retreat* and *defend*) and three different vegetation proposals (none, current, and abundant). This yielded eighteen model runs in total. For a given climate scenario, the same meteorological data were used for all planning options based on the assumption that daytime intra-urban temperature variations are small. All calculations were executed in Mathworks™ Matlab® (version 2012a). With the computational resources available, it was not possible to store the results for all model runs for every hour, so statistics were

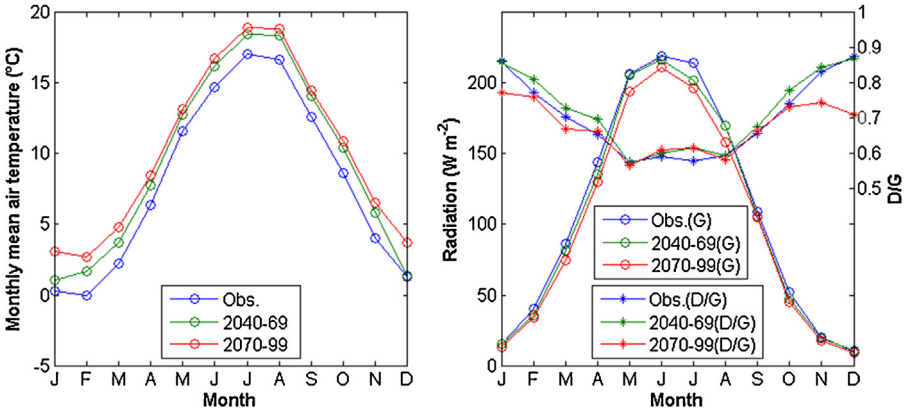

Fig. 3. Monthly average air temperature, global radiation (G), and cloudiness represented as the ratio between diffuse and global shortwave radiation (D/G) in Gothenburg between 10 a.m. and 2 p.m. for the observation period 1983–2005 (Obs.) and scenarios for mid-century (2040–2069) and the end of the century (2070–2099). The climate scenarios are derived from ECHAM5/MPI-OM GCM forced with the SRES A1B scenario (see text for further explanation).

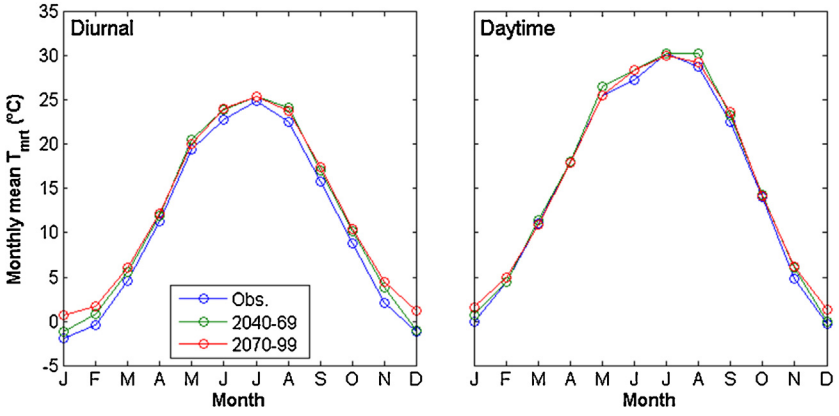

Fig. 4. Monthly averages of full-diurnal (left) and daytime-only (right) mean radiant temperature (T_{mrt}) in Gothenburg for the observed period 1983–2005 (Obs.) and for the future scenarios 2040–2069 and 2070–2099.

calculated within the model runs (as described below). Maps were generated and additional spatial analyses were performed using QGIS version 2.X and ArcGIS version 10.X.

Previous work has shown that high values of T_{mrt} at a generic urban location ($T_{mrt\ (generic)}$, see Section 2.4) are associated with measurable heat-stress effects. Thorsson et al. (2014) showed that the relative risk of heat-related deaths in Stockholm, Sweden, increased by 5% for the eldest population (80+ years) when $T_{mrt\ (generic)}$ reached 55.5 °C and by 10% when $T_{mrt\ (generic)}$ reached 59.4 °C. For all age groups, a 5% risk threshold of 57.1 °C was found. In this study, we concentrated on the spatial characteristics of T_{mrt} when $T_{mrt\ (generic)} > 55$ °C or ≥ 60 °C, which represent times of 'moderate' and 'severe' heat stress, respectively.

3. Results

This section presents the observed and projected future changes in climate (air temperature and global radiation) and T_{mrt}. The results are presented first for a generic urban location (Section 3.1), and then the spatial T_{mrt} results for the various planning strategies are presented (Section 3.2).

3.1. Climate scenarios for air temperature, global shortwave radiation, cloudiness, and T_{mrt}

Fig. 3 shows the monthly averages of hourly air temperature, daytime cloudiness, and global radiation and how these parameters change in the future under the climate change scenarios described in Section 2.3. Air temperature increased throughout the year (Fig. 3, left). The largest changes occurred already by mid-century (2040–69) for most months except for some winter months (e.g., December and January). For the end of the century scenario (2070–2099), January had the largest increase in air temperature (2.9 °C). The increase in air temperature during the summer months (June, July, and August), when heat stress mainly occurs, was 1.9 °C. Global radiation decreased, especially during the spring and summer months (Fig. 3, right). Analysis of the raw RCM outputs suggests that this decrease was due to increased daytime cloudiness. In this study, cloudiness was indicated as the ratio between the diffuse and global components of solar radiation.

The changes in T_{mrt} for the future scenarios are shown in Fig. 4. These are results for a generic urban location from SOLWIEG1D (Section 2.4). When averaging over both day and night (Fig. 4, left), an annual average increase of 1.6 °C in T_{mrt} was found at the end of the century. Even though the scenarios showed a significant increase in air temperature during the warmer months (≈2 °C), the daytime T_{mrt} did not increase noticeably (Fig. 4, right). A small increase in daytime T_{mrt} was found for June (0.8 °C) and August (0.5 °C). July, which had the highest average daytime T_{mrt} for the observed period, did not experience higher daytime T_{mrt} in the future scenario. During the middle of the century, an increase of T_{mrt} in August was evident compared with today's climate (1.5 °C). Increases in daytime T_{mrt} during the winter months were evident, and these were mainly due to increased winter air temperatures at the end of the century.

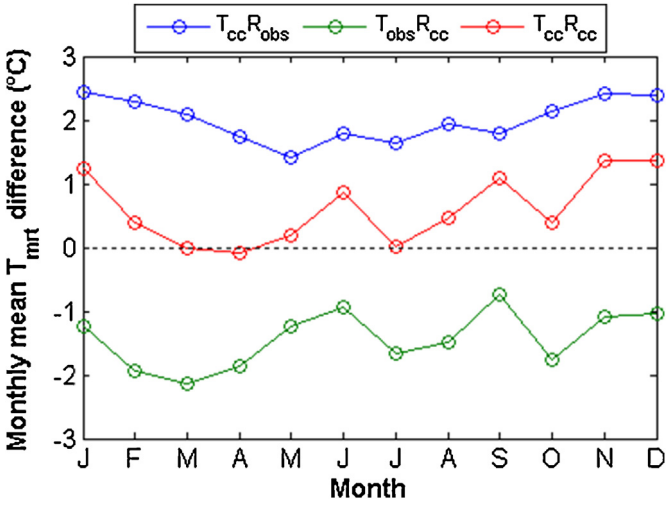

Fig. 5. Difference in average monthly daytime-only mean radiant temperature (T_{mrt}) between observed T_{mrt} and calculated T_{mrt} using the 2070–2099 scenario air temperature with observed shortwave radiation ($T_{cc}R_{obs}$); the observed air temperature with the 2070–2099 scenario radiation ($T_{obs}R_{cc}$); and the 2070–2099 scenario ($T_{cc}R_{cc}$).

To examine the sensitivity of T_{mrt} to the changes in the components within the climate scenarios used in this paper, T_{mrt} was calculated for the hybrid datasets $T_{cc}R_{obs}$ (which combined the T_a from the 2070–2099 scenario with the observed solar radiation components) and $T_{obs}R_{cc}$ (which combined the observed T_a and the shortwave radiation components from the 2070–2099 scenario). The differences between daytime T_{mrt} calculated from observations and T_{mrt} calculated with the hybrid datasets and scenario data ($T_{cc}R_{cc}$) are shown in Fig. 5. The T_{mrt} calculated using 2070–2099 T_a and observed R ($T_{cc}R_{obs}$, blue line in Fig. 5) was higher than observed for all months, whereas T_{mrt} calculated using 2070–2099 shortwave radiation and observed T_a ($T_{obs}R_{cc}$, green line in Fig. 5) was lower than observed throughout the year. The actual 2070–2099 scenario ($T_{cc}R_{cc}$, red line in Fig. 5) showed smaller changes in T_{mrt} than either of the hybrid datasets.

The monthly distribution of hourly values of daytime T_{mrt} for the observed period (1983–2005) can be found in Fig. 9 in Lindberg et al. (2013). The distribution of daytime T_{mrt} for the end of the century was very similar, and, therefore, not shown. Periods with high T_{mrt} – which indicate weather situations associated with heat stress – continued to occur during the summer months (JJA), mainly from midday to late afternoon. There were, on average, 17 days per year with $T_{mrt} > 55\,^{\circ}C$ in both the observed dataset and the 2070–2099 scenario dataset. There were 0.8 days per year and 1.3 days per year with $T_{mrt} > 60\,^{\circ}C$ for the observed and 2070–2099 scenarios, respectively.

3.2. *Spatial characteristics of* T_{mrt}

3.2.1. *Average daytime* T_{mrt} *and* T_{mrt} *during heat-stress conditions*

The average daytime T_{mrt} for each pixel for the *defend* and *retreat* planning strategies modeled with the current climate with no vegetation are shown in Fig. 6a and b. The highest average daytime values of T_{mrt} were found for open and generally sunlit locations.

The corresponding T_{mrt} averages during moderate heat-stress conditions (the hours when $T_{mrt\ (generic)}$ is $\geq 55\,^{\circ}C$) are shown in Fig. 6c and d. In contrast to Fig. 6a and b, the spatial patterns of T_{mrt} closely resembled the shadow patterns that occur during early afternoon (given that the areas northeast of building bodies were cooler due to the buildings' shadows). The reducing effect of shadowing on T_{mrt} could be seen on the northwest side of building bodies, which shows that $T_{mrt\ (generic)} > 55\,^{\circ}C$ also occurs before and around noon. Under severe heat-stress conditions ($T_{mrt\ (generic)} > 60\,^{\circ}C$), the northwest areas close to building bodies also showed high T_{mrt} (Fig. 6e and f) because hours with $T_{mrt\ (generic)} > 60\,^{\circ}C$ almost exclusively occur during the afternoon hours (2–4 p.m.). Furthermore, a general increase in T_{mrt} of about 3–6 °C was found compared to moderate heat stress conditions.

These results show that, under heat-stress conditions, high T_{mrt} is found in both open areas as well as in courtyards and even some street canyons. The latter areas are not identified as areas with high T_{mrt} based on the overall daytime averages.

3.2.2. T_{mrt} *hotspots during heat-stress conditions*

Another way to identify areas vulnerable to heat stress within the study area is to take the average of the highest 10% of T_{mrt} values during heat-stress conditions (e.g. when $T_{mrt\ (generic)} \geq 60\,^{\circ}C$). In this study, we call such figures "hotspot" maps. The procedure to generate such maps is to first identify all the hours when $T_{mrt\ (generic)} \geq 60^{\circ}$. For each of these hours, the 10% highest T_{mrt} pixel values are identified and kept, and all other pixel values are set to zero. The occasions when pixels are set to zero are included in order to compare the pixels throughout the time period being investigated. At the end of a model run, an average of all of the maps is calculated. The values in hotspot maps are not actual values of T_{mrt} and should be interpreted as an ordinal scale (i.e., hot, hotter, and hottest).

Hotspot maps for the *defend* and *retreat* planning strategies assuming the current climate with no vegetation are shown in Fig. 7. Hotspots are mainly located close to sun-exposed walls facing southwest.

The spatial distributions of T_{mrt} during warm and clear weather situations in future climates when severe heat stress is likely to occur (e.g. $T_{mrt\ (generic)} > 60\,^{\circ}C$) were almost identical to the observed climate period (Table 2) and, therefore, are not shown. These results indicate that the spatial patterns found in the observed data representing today's climate are applicable to future scenarios based on the methodology used in this paper.

3.2.3. *Effects of vegetation*

Fig. 8 shows the effects of the different vegetation proposals on the spatial distribution of T_{mrt} for the *defend* planning strategy. T_{mrt} is reduced close to each vegetation unit i.e. where the shadows from vegetation lie. Thus, vegetation units located in the shadows of buildings or ground topography do not reduce T_{mrt} during heat-stress conditions.

The reduction of average T_{mrt} for the conventional and abundant vegetation proposals (compared with the no-vegetation proposal) in Fig. 8 shows an almost linear decrease in T_{mrt} (Table 2) relative to the vegetation cover ratio (Table 1), whereas the variation (the standard deviation) increases within the study area (Table 2). For the *defend* planning strategy, the reduction in average T_{mrt} was an almost linear function of the vegetation cover fraction (Fig. 9, upper left). However, this was not true for the *retreat* planning strategy where there was a much larger difference in T_{mrt} between the no-vegetation and conventional vegetation proposals than between the conventional and abundant proposals. The same pattern was also found for hours with very high T_{mrt} ($T_{mrt\ (generic)} > 60\,^{\circ}C$) (Fig. 9, upper right). Comparing other geometry-related quantities, such as shadow patterns and number of sunlit hours per year, the same patterns were seen; vegetation was more effective in more open settings (Fig. 9, lower part). In fact, T_{mrt} (upper rows in Fig. 9) can be modeled quite well as a linear function of SVF and the number of sunlit hours (not shown).

In order to obtain a clearer picture of the spatial variations within the study area, a pixel-by-pixel comparison was performed. Fig. 10 shows the relationships between average daytime T_{mrt} and

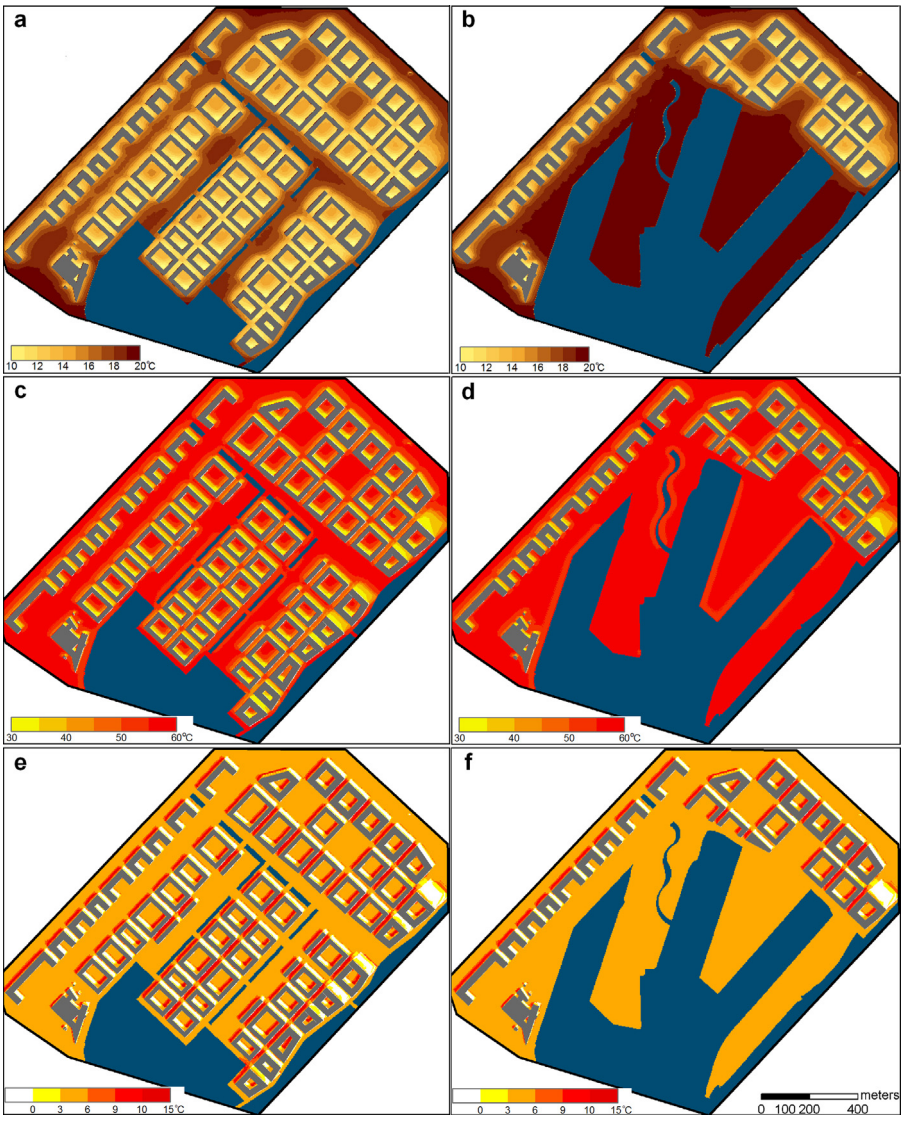

Fig. 6. Pixel-based average hourly mean radiant temperature (T_{mrt}) for (a) daytime occasions for the *defend* planning strategy, (b) daytime occasions for the *retreat* planning strategy, (c) $T_{mrt\ (generic)} > 55\,^{\circ}C$ (*defend*), (d) $T_{mrt\ (generic)} > 55\,^{\circ}C$ (*retreat*), (e) $T_{mrt\ (generic)} > 60\,^{\circ}C$ (*defend*), shown as differences from $T_{mrt\ (generic)} > 55\,^{\circ}C$ (*defend*), and (f) $T_{mrt\ (generic)} > 60\,^{\circ}C$ (*retreat*), shown as differences from $T_{mrt\ (generic)} > 55\,^{\circ}C$ (*retreat*). All figures are based on calculations with the observed climate and no vegetation. (For interpretation of the references to colour in this figure legend, the reader is referred to the web version of this article.)

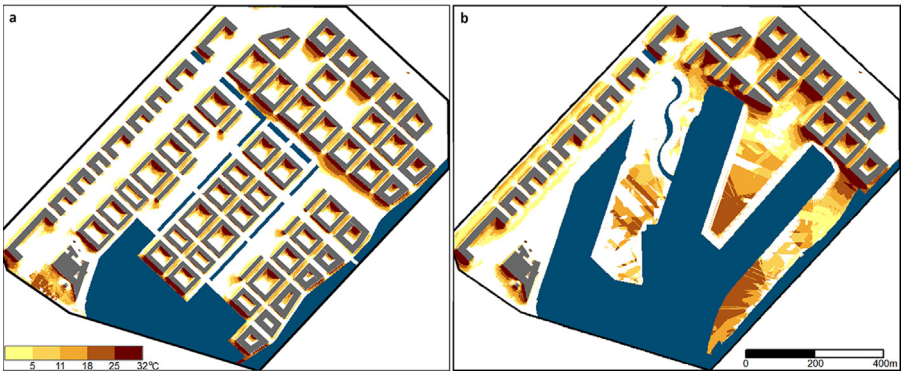

Fig. 7. Spatial variation of mean radiant temperature (T_{mrt}) hotspots defined as the 10% highest pixels when $T_{mrt\ (generic)} > 60\,^{\circ}C$ for (a) the *defend* planning strategy without vegetation and (b) the *retreat* planning strategy without vegetation. For further explanation of the legend, see the text. Observation data (1983–2006) representing the climate of today is used. (For interpretation of the references to colour in this figure legend, the reader is referred to the web version of this article.)

SVF as well as shadow pattern for individual pixels for the *defend* strategy. There was a positive correlation between daytime T_{mrt} and SVF, with the highest T_{mrt} associated with open areas (Fig. 10a). In areas with lower SVF, such as street canyons and courtyards,

Table 2
Basic statistics for the different planning proposals and climate scenarios used in this study. Results are shown as the mean and standard deviation (SD).

DEFEND	Observations						2070–2099					
	Vegetation strategy						Vegetation strategy					
	None		Conventional		Abundant		None		Conventional		Abundant	
	Mean	SD	Mean	SD	Mean	SD	Mean	SD	Mean	SD	Mean	SD
T_{mrt} *diurnal*	6.9	0.6	7.1	0.7	7.4	1.1	8.8	0.5	9.0	0.7	9.4	1.1
T_{mrt} *daytime*	15.9	2.6	15.5	2.4	15.1	2.3	17.2	2.3	16.8	2.1	16.5	2.0
$T_{mrt} > 55\,^{\circ}C_{daytime}$	26.7	2.7	26.1	2.5	25.4	2.5	28.4	2.7	27.8	2.5	27.1	2.5
$T_{mrt} > 60\,^{\circ}C_{daytime}$	30.8	2.8	30.1	2.6	29.4	2.7	31.8	2.8	31.1	2.6	30.4	2.7
$T_{mrt} > 55\,^{\circ}C_{hour}$	51.0	7.3	49.5	7.4	47.3	8.1	51.5	6.9	50.1	6.9	47.9	7.6
$T_{mrt} > 60\,^{\circ}C_{hour}$	55.7	8.5	54.2	8.9	52.1	9.7	55.9	8.1	54.5	8.5	52.4	9.3
$T_{mrt} > 55\,^{\circ}C_{(hours/year)}$	45.9	35.4	34.4	32.8	27.9	32.0	67.1	50.7	50.5	46.9	40.8	45.9
$T_{mrt} > 60\,^{\circ}C_{(hours/year)}$	4.4	6.5	2.9	5.9	2.4	5.5	8.9	12.6	5.9	11.4	4.8	10.7
$Shadow_{(hours/year)}$	2215	1087	1953	1057	1656	1091	2215	1087	1953	1057	1656	1091
$SVF_{buildings}$	0.76	0.19	0.76	0.19	0.76	0.19	0.76	0.19	0.76	0.19	0.76	0.19
$SVF_{buildings+vegetation}$	0.76	0.19	0.69	0.20	0.61	0.25	0.76	0.19	0.69	0.20	0.61	0.25
Retreat	Mean	SD	Mean	SD	Mean	SD	Mean	SD	Mean	SD	Mean	SD
T_{mrt} *diurnal*	7.0	0.4	7.4	0.9	7.7	1.2	8.8	0.4	9.2	0.8	9.5	1.2
T_{mrt} *daytime*	18.6	2.6	17.7	2.3	17.3	2.3	19.6	2.3	18.7	2.0	18.4	2.0
$T_{mrt} > 55\,^{\circ}C_{daytime}$	28.8	2.2	27.7	2.3	27.0	2.5	30.5	2.2	29.4	2.3	28.7	2.5
$T_{mrt} > 60\,^{\circ}C_{daytime}$	32.9	2.3	31.8	2.4	31.1	2.6	33.9	2.3	32.8	2.4	32.1	2.6
$T_{mrt} > 55\,^{\circ}C_{hour}$	54.1	5.1	51.9	6.4	50.1	7.7	54.8	4.9	52.5	6.0	50.7	7.3
$T_{mrt} > 60\,^{\circ}C_{hour}$	58.6	5.8	56.4	7.4	54.6	8.7	58.8	5.6	56.6	7.1	54.8	8.4
$T_{mrt} > 55\,^{\circ}C_{(hours/year)}$	90.5	44.8	51.5	38.3	40.5	35.6	90.5	44.8	76.1	54.5	60.5	51.4
$T_{mrt} > 60\,^{\circ}C_{(hours/year)}$	14.9	10.9	5.7	7.2	3.9	5.9	28.2	19.7	11.6	14.1	8.2	11.9
$Shadow_{(hours/year)}$	3337	1032	2758	981	2420	1070	3337	1032	2758	981	2420	1070
$SVF_{buildings}$	0.90	0.15	0.90	0.15	0.90	0.15	0.90	0.15	0.90	0.15	0.90	0.15
$SVF_{buildings+vegetation}$	0.90	0.15	0.80	0.20	0.72	0.25	0.90	0.15	0.80	0.20	0.72	0.25

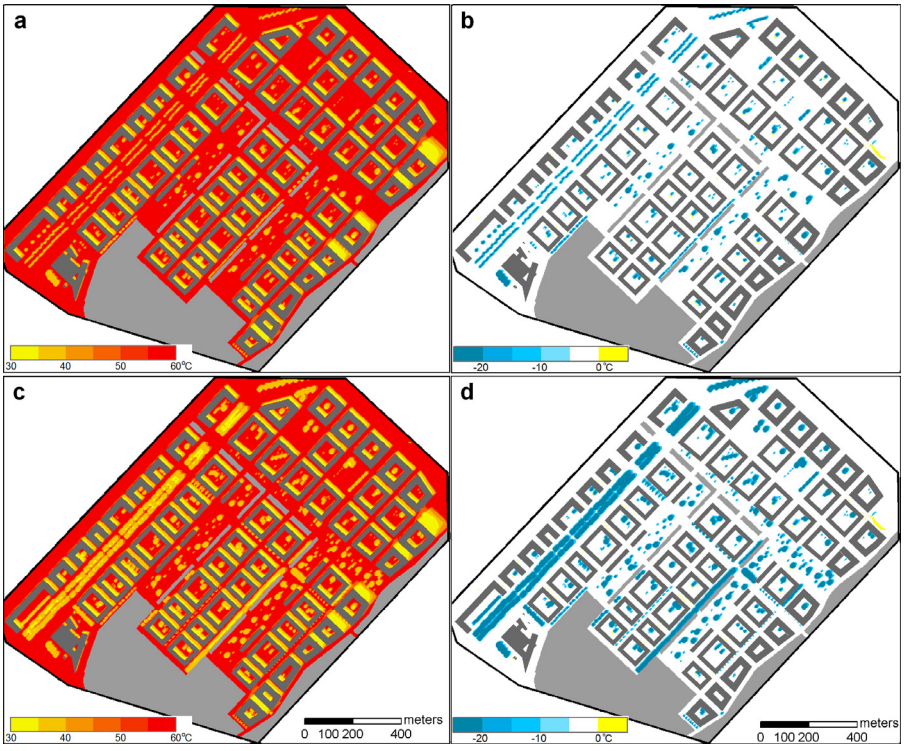

Fig. 8. (a) The average mean radiant temperature (T_{mrt}) for hours with $T_{mrt\ (generic)} > 60\,^{\circ}C$ and the *defend* planning strategy with conventional vegetation. (b) The difference between (a) and the corresponding calculation with no vegetation. (c) The average T_{mrt} for hours with $T_{mrt\ (generic)} > 60\,^{\circ}C$ and the *defend* planning strategy with abundant vegetation. (d) The difference between (c) and the corresponding calculation with no vegetation. All maps are based on today's climate. (For interpretation of the references to colour in this figure legend, the reader is referred to the web version of this article.)

there was a considerable range of T_{mrt} due to shading effects. Higher T_{mrt} values were confined to south-facing building walls, which are more exposed to incoming solar radiation during the daytime. The highest range was found around SVF = 0.6. These locations are found either close to north-facing walls and experience very low averages of T_{mrt} or close to south-facing walls where the average T_{mrt} could be very high. Under the conventional vegetation approach, a similar pattern was observed except for the high T_{mrt} observed in areas with very low SVF (Fig. 10b). Such high T_{mrt} was found in sunlit areas underneath tree canopies due to the blockage of relatively cooler

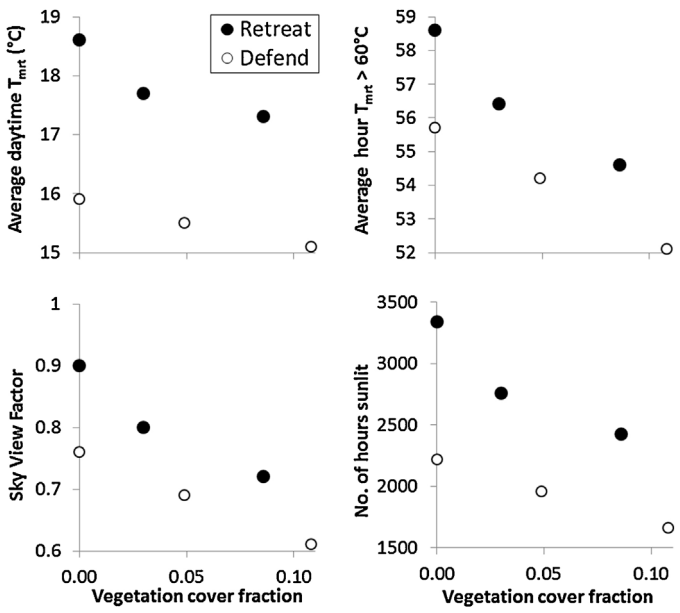

Fig. 9. The average effects of vegetation cover fraction. Upper left: average values of daytime mean radiant temperature (T_{mrt}). Upper right: average T_{mrt} when $T_{mrt\ (generic)} > 60\,^{\circ}C$. Lower left: sky view factor. Lower right: number of hours of sunlit ground.

sky and increased longwave radiation from the trees. As shown in Fig. 10c and d, scatterplots between T_{mrt} and shadow pattern further confirmed the strong effect of shadow on the magnitude of the average daytime T_{mrt} ($R^2 = 0.97$). Unlike SVF, low T_{mrt} values were found in areas under shadow most of the time. The correlation with shadow pattern was even stronger ($R^2 = 0.99$) for hours with $T_{mrt\ (generic)} > 60\,^{\circ}C$.

3.2.4. Distance to nearest shaded area

Another technique to visualize the spatial distribution of outdoor heat stress vulnerability within an urban neighborhood is to calculate the pixel-wise distance from high T_{mrt} (especially unshaded) locations to the nearest 'cool' (low T_{mrt}; in shade) area. A threshold of $T_{mrt} = 57\,^{\circ}C$ was used to identify 'warm' (sunlit) areas. The maps were calculated using a cost-distance algorithm in ArcGIS version 10.1. Buildings and water were treated as impenetrable barriers.

The distance to the nearest shaded area during severe heat-stress conditions ($T_{mrt\ (generic)} > 60\,^{\circ}C$) for the *retreat* planning strategy is shown in Fig. 11 for three vegetation proposals under the observed climate. With no vegetation (Fig. 11a), the three piers had very large distances to shaded areas due to a complete lack of nearby shaded locations. Within the built-up areas in the northwest and northeast of the study area, higher diversity and lower distances to shaded areas were found. Comparing the hotspot map in Fig. 7b with Fig. 11 shows some areas that are both hotspots and have relatively long distances to cool areas. These are most notably on the piers but are also near the middle of southwest-facing walls.

4. Discussions

As shown in Fig. 4, the changes in T_{mrt} for the future scenarios are moderate. This is because the increase in air temperature during the warmer months (≈2 °C) in the future scenarios is counterbalanced by a decrease in solar radiation (an increase in cloudiness). Increases in daytime T_{mrt} during the winter months are evident, mainly due to increased winter air temperatures at the end of the century.

The sensitivity analysis of outputs from the climate scenarios on T_{mrt} shows that both air temperature and global radiation have a large effect on T_{mrt}. Sensitivity of T_{mrt} due to changes in humidity were not analyzed here because earlier studies demonstrated that T_{mrt} is unaffected by changes in humidity (Onomura, Grimmond, Lindberg, Holmer, & Thorsson, 2015).

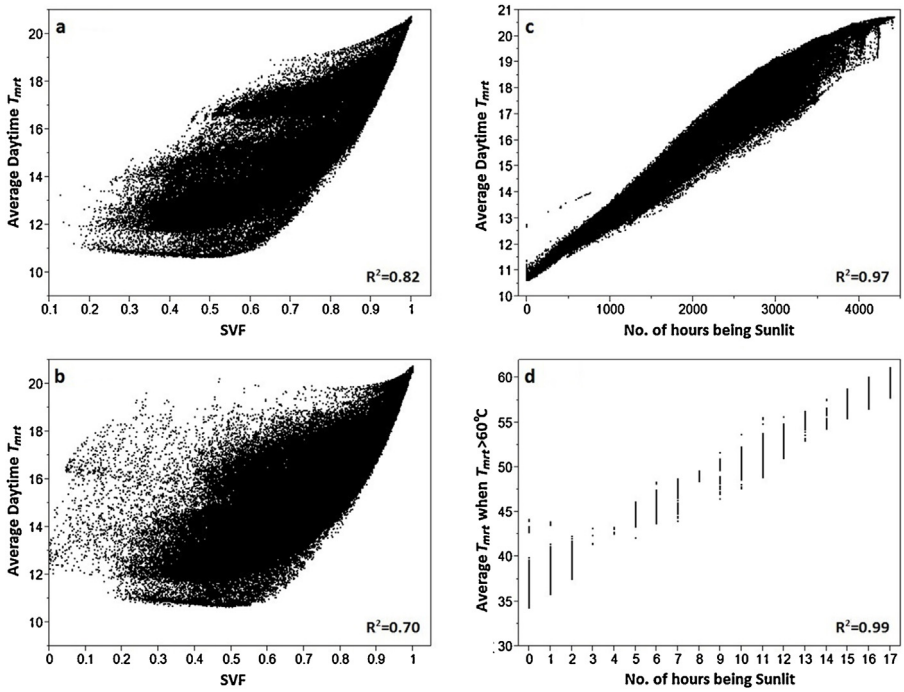

Fig. 10. Scatterplots between average daytime mean radiant temperature (T_{mrt}) and SVF for (a) the no-vegetation and (**b**) the conventional vegetation approach. The effect of shadow pattern on (**c**) average daytime T_{mrt} and (d) average hourly T_{mrt} when $T_{mrt\ (generic)} > 60\,^{\circ}C$ based on the *defend* strategy.

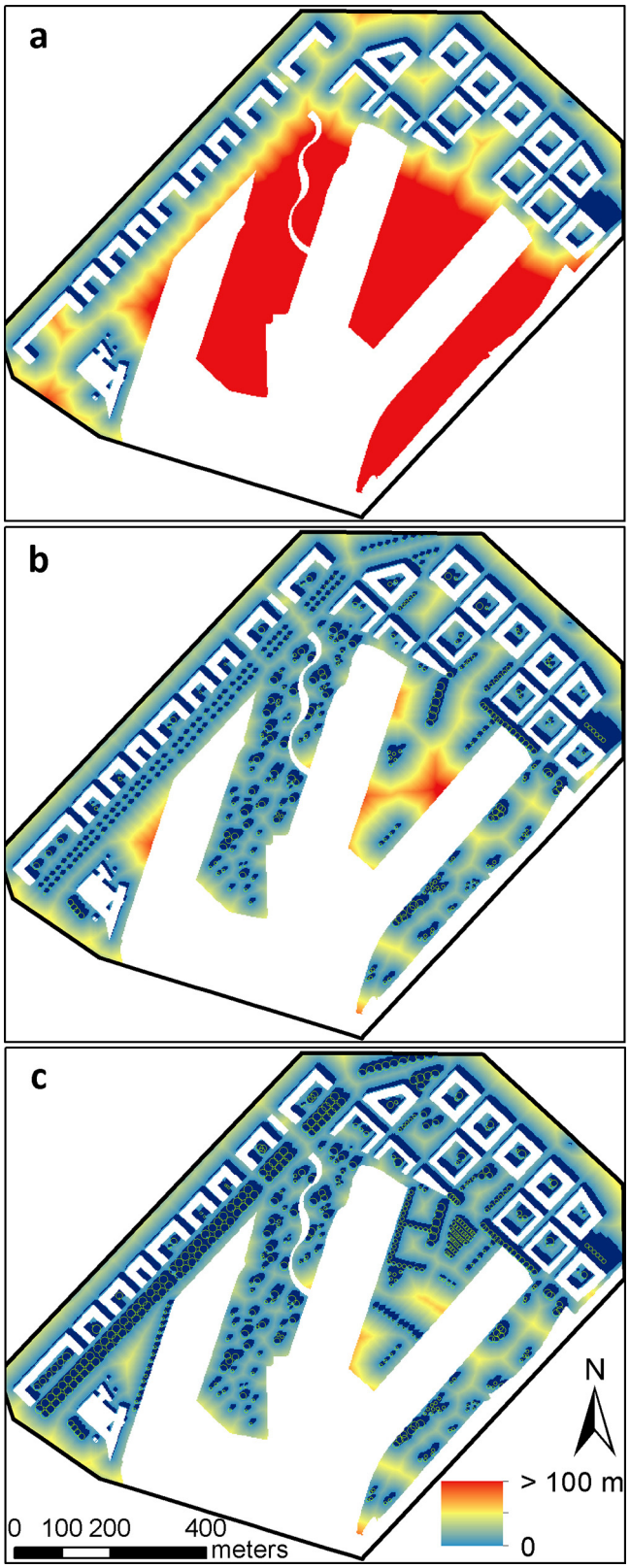

Fig. 11. Distance to the nearest shaded pixel when $T_{mrt\ (generic)} > 60\,^{\circ}C$ using the observed climate and (a) no vegetation, (b) conventional vegetation, and (c) abundant vegetation. Green circles are the positions and extents of the vegetation units. (For interpretation of the references to colour in this figure legend, the reader is referred to the web version of this article.)

Regarding the spatial variability of T_{mrt}, this study shows that the single most effective measure for reducing T_{mrt} in urban areas during warm and clear daytime weather situations is providing shadow to reduce incoming shortwave radiation. This has also been acknowledged in other studies (e.g. Ketterer & Matzarakis 2014; Lee, Holst, & Mayer, 2013; Thorsson et al., 2014).

As shown in Fig. 7, T_{mrt} hotspots are mainly located close to sun-exposed, southwest-facing walls. This has three main explanations. First, high longwave radiation fluxes originate from the warm building walls. Second, the cooler sky is partly blocked by the same buildings. Third, reflected shortwave radiation fluxes are greater close to sunlit building walls. In the open locations, less building wall and more of the cool sky is visible. Open areas, which were shown in Fig. 6 to have high average T_{mrt}, are not usually identified as hotspots. There are exceptions, however, for the *retreat* planning strategy (Fig. 7b) where open areas with SVF ≈ 1 can be hotspots. This might occur during hot and partly cloudy situations when the diffuse shortwave radiation from the visible sky increases T_{mrt}. This effect can also be seen in the western corner of the study area in Fig. 7a. However, such locations are rare in the *defend* strategy, and the warmest areas are usually located close to sunlit walls that face southwest. The location of T_{mrt}-related hotspots has also been identified by Lindberg et al., 2013.

Because shadow patterns have a very large effect on the spatial patterns of T_{mrt} during the warm and clear weather situations when heat stress is most likely to occur, vegetation (trees and bushes) is an effective measure to reduce T_{mrt} (e.g. Shashua-Bar & Hoffman 2000; Lee et al., 2013). As shown in Fig. 8, the reduction of T_{mrt} is located very close to each vegetation unit, i.e., where shadows from vegetation are found. This has also been seen in other studies (e.g. Lindberg et al., 2013; Thorsson et al., 2014). Although the reduction in T_{mrt} from each vegetation unit is determined by the size and shape of the unit, Fig. 9 shows that the reduction in the average of T_{mrt} over the whole study area from increasing the vegetation cover fraction also depends on the building density and the fraction of sunlit area. This indicates that introducing vegetation in areas with low building density (higher SVF) reduces T_{mrt} more effectively than introducing vegetation into a dense urban setting. The scatterplots shown in Fig. 10 show the strong relationship between shadow and T_{mrt}. This suggests that optimizing urban geometry also has a great potential for improving outdoor thermal comfort by providing shade during heat-stress conditions.

The distance to the nearest shaded cool area during severe heat stress conditions ($T_{mrt\ (generic)} > 60\,^{\circ}C$) for the *retreat* planning strategy, as shown in Fig. 11, can be used to identify areas where vulnerability to heat stress during clear and warm weather situations might be high and could, therefore, be useful for identifying areas where measures could be taken for reducing heat stress. It is often argued that including a diverse range of environments in a neighborhood can accommodate a range of wishes and demands from individuals regarding thermal comfort (Katzschner, 2006; Thorsson, Lindqvist, & Lindqvist, 2004).

Our findings suggest that dense urban structures reduce outdoor heat stress. This agrees with previous studies, which have shown that urban layout plays an important role in determining heat-related health effects (Katzschner, 2010; Stone, Hess, & Frumkin, 2010). However, the effects of heat-stress and the need for adaptation measures from a climate-change perspective are seldom considered by urban planners (Bernard & McGeehin, 2004; Bulkeley, 2010). Possible reasons for this include limited knowledge about heat stress and poor interaction between knowledge producers (generally scientists) and urban planners (Runhaar, Mees, Wardekker, van der Sluijs, & Driessen, 2012). While the impacts of heat stress are often considered in high-level planning activities (Sherwood & Huber, 2010; Willett & Sherwood, 2010; Dugord, Lauf, Schuster, & Kleinschmit, 2014), the present study provides insights

whereby urban planners and designers can mitigate heat stress by designing better neighborhoods at the microclimatic scale. This study extends the work of Thorsson et al. (2011) by incorporating vegetation into the modeling of outdoor heat stress for temperate climates. The results suggest that vegetation is an effective measure to mitigate the effects of climate change on outdoor heat stress.

In conclusion, two approaches are recommended to reduce summer outdoor heat stress in high-latitude cities: increase the amount of urban greenery and increase the building density, i.e. prefer high and dense building structures. Also, adding vegetation increases the latent heat fluxes through evapotranspiration and thus helps reduce air temperature, especially in areas with no or little existing vegetation where it also produces a larger cooling effect than adding vegetation to already highly vegetated areas (Loridan & Grimmond, 2012). It should be stressed that increasing urban density without increasing the amount of vegetation could have a positive feedback on heat stress due to increased nighttime temperatures due to urban heat island effects.

Additional recommendations are:

- Trees are to be preferred over lower vegetation such as bushes and grass because trees are able to produce more extensive areas of shadow.
- Trees should be placed in sunlit areas with no or little vegetation where they can contribute to shading.
- Deciduous trees are to be preferred over evergreen trees because they give shade in summer and allow solar radiation to penetrate in winter.
- Species choice, location, and shape of the vegetation must be considered in order to minimize problems such as reduced security, reduced indoor light, maintenance, damage to underground infrastructure, etc.

4.1. Limitations and uncertainties

There are a number of limitations that should be taken into account when interpreting the results and drawing conclusions from this kind of study. The model simulation results are conditional on the urban setting used, which in this case has a clear directionality with streets and buildings aligned along northwest – southeast and southwest – northeast axes. This directionality accentuates the view that southwest-facing walls are prone to potential heat stress. Future research will include studies using generic urban geometrical forms such as circular courtyards, regular urban canyons in various directions, etc. Furthermore, this study only models the future climate using one climate scenario, whereas it would be preferable to investigate the effect of climate change on future T_{mrt} using outputs from various GCMs/RCMs and emission scenarios. Although not within the scope of this paper, studies based on multiple GCM/RCM combinations will be conducted within the 'Adapting cities to climate induced risk' project.

This study focuses on T_{mrt}, which covers only one aspect of the human energy balance and thus is an incomplete description of thermal comfort. Nevertheless, this study mainly focuses on heat stress during hot and clear weather where T_{mrt} has been shown to be one of the most important meteorological parameters affecting outdoor thermal comfort (e.g. Mayer et al., 2008).

One important parameter for human thermal comfort and outdoor heat stress that was not included in this study is wind. Wind affects thermal comfort in two ways. First, wind contributes to convective cooling of the human body, which can reduce the heat load and thus reduce the risk of heat stress (Saneinejad, Moonen, & Carmeliet, 2014; Toparlar et al., 2015). Second, advection of air at the local scale can alter the overall thermal environment (Brandsma, Können, & Wessels, 2003; Harman & Belcher, 2006). To obtain spatial information on near-ground wind speed at the same spatial resolution as SOLWEIG (2 m), 3D computational fluid dynamical modeling is often used. This is a computationally intensive method that requires extensive computer resources and is time consuming. Work is currently being done to develop a 2D statistical wind model that could be used in studies similar to the one presented here (Johansson 2012; Johansson et al., 2016).

Another factor that could have been included is a description of the material composition of the ground and walls because these affect radiative fluxes via albedo and emissivity, both shortwave and longwave. However, recent research has indicated that materials of different albedo have only a minor effect on outdoor thermal comfort (Erell, Pearlmutter, Boneh, & Kutiel, 2014). Different ground surfaces could affect the radiant environment and thus T_{mrt}. However, the outgoing shortwave and longwave fluxes that are affected by the ground surface are relatively small compared to the incoming fluxes and to fluxes originating from the four cardinal points (see Fig. 10 in Lindberg et al., 2013). That said, altering the ground material also affects the local climate via sensible and latent energy fluxes, and this affects air temperature that in turn alters T_{mrt}. However, this study considers heat stress during the daytime when turbulent mixing and advection even out differences in air temperature on the local scale, so this effect is probably small. There is no land-cover scheme included in the current version of the SOLWEIG model.

This study showed that reducing the radiant component of T_{mrt} by creating shade is an effective measure for reducing T_{mrt} and, therefore, for mitigating potential outdoor heat stress. However, it is also important to recognize the unwanted effects of creating too much shadow. During winter, high-latitude locations such as Gothenburg benefit from direct sunshine, which reduces both outdoor cold stress and energy use for heating. Therefore, the locations of trees should be considered thoughtfully so as to minimize unwanted shadowing during non heat-stress weather situations. Thus deciduous trees that allow solar radiation through the tree canopy during winter are preferred (Konarska et al., 2014).

5. Conclusions

The spatial pattern of outdoor T_{mrt} during heat-stress conditions is very different from the average daytime T_{mrt} pattern. Whereas average daytime T_{mrt} is lower around buildings and higher in open areas, T_{mrt} under heat-stress conditions is highest near sunlit building walls, including walled-in courtyards and narrow street canyons. Including trees in the urban setting thus seems to be the most effective measure for reducing T_{mrt} during heat-stress conditions. We found that the average T_{mrt} across the whole study area during heat-stress conditions declined almost linearly as a function of increasing vegetation cover fraction. This was not always the case for the overall daytime average T_{mrt}, where in one scenario (*retreat*) there was little change in average T_{mrt} between conventional and abundant vegetation scenarios. The simulated average daytime T_{mrt} for the future scenarios was not higher than for the current climate even though air temperature was higher. The increased longwave radiation flux caused by the higher temperature was counterbalanced by reduced shortwave radiation fluxes caused by increased cloudiness. The spatial pattern of outdoor T_{mrt} was also similar in the future scenarios compared to today's conditions.

In our study, the direct effect of trees in reducing T_{mrt} under heat-stress conditions is spatially restricted to the areas of shadow they create and is thus related to the size of the vegetation units and the number of vegetation units. However, when assessing vulnerability to heat stress using spatial maps of the distance to the nearest shaded pixel, the size of the vegetation units is unimportant but their location is critical. Trees in open areas reduce potential vul-

nerability for the entire surrounding area, whereas trees in sunlit locations near to buildings provide less benefit.

References

ASHRAE. (2001). *ASHRAE fundamentals handbook 2001* (SI ed.). American Society of Heating, Refrigerating, and Air-Conditioning Engineers.

Ali-Toudert, F., & Mayer, H. (2007). Thermal comfort in an east-west oriented street canyon in Freiburg (Germany) under hot summer conditions. *Theoretical and Applied Climatology*, *87*, 223–237.

Bernard, S. M., & McGeehin, M. A. (2004). Municipal heat wave response plans. *American Journal of Public Health*, *94*(9), 1520–1522.

Brandsma, T., Können, G. P., & Wessels, H. R. A. (2003). Empirical estimation of the effect of urban heat advection on the temperature series of De Bilt (The Netherlands). *International Journal of Climatologyb*, *23*(7), 829–845.

Bulkeley, H. (2010). Cities and the governing of climate change. *Annual Review of Environment and Resources*, *35*(1), 229–253.

Crawford, T. M., & Duchon, C. E. (1999). An improved parameterization for estimating effective atmospheric emissivity for use in calculating daytime downwelling longwave radiation. *Journal of Applied Meteorology*, *38*, 474–480.

Dugord, P. A., Lauf, S., Schuster, C., & Kleinschmit, B. (2014). Land use patterns, temperature distribution, and potential heat stress risk – The case study Berlin, Germany Computers. *Environment and Urban Systems*, *48*, 86–98.

Emmanuel, R., & Fernando, H. J. S. (2007). Urban heat islands in humid and arid climates: role of urban form and thermal properties in Colombo, Sri Lanka and Phoenix, USA. *Climate Research*, *34*, 241–251.

Erell, E., Pearlmutter, D., Boneh, D., & Kutiel, P. B. (2014). Effect of high-albedo materials on pedestrian heat stress in urban street canyons. *Urban Climate*, *10*, 367–386.

Fiala, D., Havenith, G., Bröde, P., Kampmann, B., & Jendritzky, G. (2012). UTCI-Fiala multi-node model of human heat transfer and temperature regulation. *International Journal of Biometeorology*, *56*, 429–441.

Höppe, P. (1992). Ein neues verfahren zur bestimmung der mittleren strahlungstemperatur in frien. *Wetter und Leben*, *44*, 147–151.

Harman, I. N., & Belcher, S. E. (2006). The surface energy balance and boundary layer over urban street canyons. *Quarterly Journal of the Royal Meteorological Society*, *132*(621), 2749–2768.

IPCC. (2007). *AR4 synthesis report, full report intergovernmental panel on climate change*. pp. 73. 73 [http://www.ipcc.ch/pdf/assessment-report/ar4/syr/ar4_syr.pdf.].

Johansson, L. (2012). *Modelling near ground wind speed in urban environments using high-resolution digital surface models and statistical methods. Master Thesis*. INES nr. 234 Lund University.

Johansson, L., Lindberg, F., Onomura, S., Holmer, B., & Thorsson, S. (2016). Towards the modelling of pedestrian wind speed using high resolution digital surface models and statistical methods. *Theoretical and Applied Climatology*, http://dx.doi.org/10.1007/s00704-015-1405-2

Jonsson, A. C., & Lundgren, L. (2014). Vulnerability and adaptation to heat in cities: perspectives and perceptions of local adaptation decision-makers in Sweden. *Local Environment*, http://dx.doi.org/10.1080/13549839.2014.896326

Katzschner, L. (2006). Microclimatic thermal comfort analysis in cities for urban planning and open space design. In *Comfort and energy use in buildings*. London: Network for Comfort and Energy use in Buildings (NCUB).

Katzschner, L. (2010). Outdoor thermal comfort under consideration of global climate change and urban development strategies. In *Proceedings of the conference: adapting to change: new thinking on comfort* (pp. 9–11) [April 2010].

Ketterer, C., & Matzarakis, A. (2014). Human-biometeorological assessment of heat stress reduction by replanning measures in Stuttgart, Germany. *Landscape and Urban Planning*, *122*, 78–88.

Kjellström, E., Bärring, L., Gollvik, S., Hansson, U., Jones, C., Samuelsson, P., et al. (2005). A 140-year simulation of European climate with the new version of the Rossby Centre regional atmospheric climate model (RCA3). In *SMHI Reports Meteorology and Climatology No. 108*. pp. 54. SE-60176 Norrköping, Sweden: SMHI.

Konarska, J., Lindberg, F., Larsson, A., Thorsson, S., & Holmer, B. (2014). Transmissivity of solar radiation through crowns of single urban trees—application for outdoor thermal comfort modelling. *Theoretical And Applied Climatology*, *117*, 363–376.

Lee, H., Holst, J., & Mayer, H. (2013). Modification of human-Biometeorologically significant radiant flux densities by shading as local method to mitigate heat stress in summer within urban street canyons. *Advances in Meteorology*, *2013*, 13.

Lindberg, F. (2005). Towards the use of local governmental 3-d data within urban climatology studies. *Mapping and Image Science*, *2*, 32–37.

Lindberg, F. (2012). *The SOLWEIG-model*. Sweden: Gothenburg University [http://www.gvc.gu.se/Forskning/klimat/stadsklimat/gucg/software/solweig/, (assessed 02.12.14.)].

Lindberg, F., & Grimmond, C. S. B. (2011). The influence of vegetation and building morphology on shadow patterns and mean radiant temperatures in urban areas: model development and evaluation. *Theoretical and Applied Climatology*, *105*, 311–323.

Lindberg, F., Holmer, B., & Thorsson, S. (2008). SOLWEIG 1.0—Modelling spatial variations of 3D radiant fluxes and mean radiant temperature in complex urban settings. *International Journal of Biometeorology*, *52*, 697–713.

Lindberg, F., Holmer, B., Thorsson, S., & Rayner, D. (2013). Characteristics of the mean radiant temperature in high latitude cities—implications for sensitive climate planning applications. *International Journal of Biometeorology*, 1–15.

Loridan, T., & Grimmond, C. S. B. (2012). Characterization of energy flux partitioning in urban environments: links with surface seasonal properties. *Journal of Applied Meteorology and Climatology*, *51*, 219–241.

Mayer, H., & Höppe, P. (1987). Thermal comfort of man in different urban environments. *Theoretical and Applied Climatology*, *38*, 43–49.

Mayer, H., Holst, J., Dostal, P., Imbery, F., & Schindler, D. (2008). Human thermal comfort in summer within an urban street canyon in Central Europe. *Meteorologische Zeitschrift*, *17*, 241–250.

McCarthy, M. P., Best, M. J., & Betts, R. A. (2010). Climate change in cities due to global warming and urban effects. *Geophysical Research Letters*, *37*, L09705.

Meehl, G. A., Covey, C., Taylor, K. E., Delworth, T., Stouffer, R. J., Latif, M., et al. (2007). THE WCRP CMIP3 multimodel dataset: a new era in climate change research. *Bulletin of the American Meteorological Society*, *88*, 1383–1394.

Meehl, G. A., & Tebaldi, C. (2004). More intense, more frequent, and longer lasting heat waves in the 21st century. *Science*, *305*, 994–997.

Moss, R. H., Edmonds, J. A., Hibbard, K. A., Manning, M. R., Rose, S. K., van Vuuren, D. P., et al. (2010). The next generation of scenarios for climate change research and assessment. *Nature*, *463*, 747–756.

Muthers, S., Matzarakis, A., & Koch, E. (2010). Climate change and mortality in Vienna–a human biometeorological analysis based on regional climate modeling. *International Journal of Environmental Research and Public Health*, *7*, 2965–2977.

Oke, T. R. (1987). *Boundary layer climates*. Cambridge: Routledge.

Onomura, S., Grimmond, C. S. B., Lindberg, F., Holmer, B., & Thorsson, S. (2015). Meteorological forcing data for urban outdoor thermal comfort models obtained from a coupled convective boundary layer and surface energy balance scheme. *Urban Climate*, *11*, 1–23.

Oudin Åström, D., Forsberg, B., Ebi, K. L., & Rocklöv, J. (2013). Attributing mortality from extreme temperatures to climate change in Stockholm, Sweden. *Nature Climate Change*, *3*, 1050–1054.

Rayner, D., Lindberg, F., Thorsson, S., & Holmer, B. (2014). A statistical downscaling algorithm for thermal comfort applications. *Theoretical and Applied Climatology*, *122*(3), 729–742.

Reindl, D. T., Beckman, W. A., & Duffie, J. A. (1990). Diffuse fraction correlation. *Solar Energy*, *45*, 1–7.

Rocklov, J., & Forsberg, B. (2008). The effect of temperature on mortality in Stockholm 1998–2003: a study of lag structures and heatwave effects. *Scandinavian Journal of Public Health*, *36*, 516–523.

Roeckner, E., Bäuml, G., Bonaventura, L., Brokopf, R., Esch, M., Giorgetta, M., et al. (2003). *The atmospheric general circulation model ECHAM5, part I: model description*. 140. Max Planck Institue for Meteorology.

Runhaar, H., Mees, H., Wardekker, A., van der Sluijs, J., & Driessen, P. P. J. (2012). Adaptation to climate change-related risks in Dutch urban areas: stimuli and barriers. *Reginoal Environmental Change*, *12*, 777–790.

SOU. (2007). Sweden facing climate—threats and opportunities. In *Final report from the swedish commission on climate and vulnerability*. Stockholm, Sweden: Swedish Government Official Report No. 60.

Saneinejad, S., Moonen, P., & Carmeliet, J. (2014). Coupled CFD, radiation and porous media model for evaluating the micro-climate in an urban environment. *Journal of Wind Engineering and Industrial Aerodynamics*, *128*, 1–11.

Shashua-Bar, L., & Hoffman, M. E. (2000). Vegetation as a climatic component in the design of an urban street: an empirical model for predicting the cooling effect of urban green areas with trees. *Energy And Buildings*, *31*, 221–235.

Sherwood, S. C., & Huber, M. (2010). An adaptability limit to climate change due to heat stress. *Proceedings of the National Academy of Sciences*, *107*, 9552–9555.

Stone, B., Hess, J. J., & Frumkin, H. (2010). Urban form and extreme heat events: are sprawling cities more vulnerable to climate change than compact cities? *Environmental Health Perspectives*, *118*(10), 1425–1428.

Thorsson, S., Lindberg, F., Bjorklund, J., Holmer, B., & Rayner, D. (2011). Potential changes in outdoor thermal comfort conditions in Gothenburg: sweden due to climate change: the influence of urban geometry. *International Journal of Climatology*, *31*, 324–335.

Thorsson, S., Lindqvist, M., & Lindqvist, S. (2004). Thermal bioclimatic conditions and patterns of behaviour in an urban park in Goteborg: sweden. *International Journal of Biometeorology*, *48*, 149–156.

Thorsson, S., Rocklöv, J., Konarska, J., Lindberg, F., Holmer, B., Dousset, B., et al. (2014). Mean radiant temperature—a predictor of heat related mortality. *Urban Climate*, *10*, 332–345.

Toparlar, Y., Blocken, B., Vos, P., van Heijst, G. J. F., Janssen, W. D., van Hooff, T., et al. (2015). CFD simulation and validation of urban microclimate: a case study for Bergpolder Zuid, Rotterdam. *Building and Environment*, *83*, 79–90.

Willett, K. M., & Sherwood, S. (2010). Exceedance of heat index thresholds for 15 regions under a warming climate using the wet-bulb globe temperature. *Int. J. Climatol.*, *32*, 161–177.

VDI, 1998. Methods for the human-biometeorological assessment of climate and air hygiene for urban and regional planning. Part I: Climate. VDI 3787, Part 2, Belin 29p.